J. Fluid Mech. (1995), *vol.* 290, *pp.* 39–66

Sedimentation and sediment flow in settling tanks with inclined walls

By B. KAPOOR† AND A. ACRIVOS

The Levich Institute, The City College of the City University of New York, New York, NY 10031, USA

(Received 5 May 1994 and in revised form 19 October 1994)

The flow of a sediment layer that forms on an inclined plate as a consequence of the steady sedimentation of spherical particles was investigated theoretically as well as experimentally. The theoretical analysis was based on the model proposed by Nir & Acrivos (1990), modified to include shear-induced diffusion due to gradients in the shear stress as well as a slip velocity along the wall due to the finite size of the particles. The resulting set of partial differential equations, which is amenable to a similarity-type solution both near the leading edge as well as far downstream, was solved numerically using a finite difference scheme thereby yielding theoretical predictions for the particle concentration and velocity profiles, plus the local sediment layer thickness, all along the plate. In addition, a new experimental technique based on laser Doppler anemometry was developed and was used to measure the particle velocity profiles in the highly concentrated sediment layer as well as the corresponding slip coefficient which relates the slip velocity to the velocity gradient adjacent to a wall. The thickness profile of the sediment layer was also measured experimentally by means of video imaging. It was found that the experimental results thus obtained for the particle velocity profile and for the local sediment layer thickness were in very good agreement with the corresponding theoretical predictions especially considering that the latter did not make use of any adjustable parameters.

1. Introduction

The separation of solid particles from liquids by means of gravity settling constitutes an important physical step in many chemical industries. This process is often slow and requires large vessels especially when the particles are small and the fluid is viscous. It has been shown, however, that the settling process can be enhanced by employing vessels with inclined walls which, for an equivalent rate of production of sediment or of clear fluid, typically occupy considerably less space than their vertical counterparts. These settlers, often called supersettlers, make use of closely spaced parallel plates.

The different regions of the flow field in a typical parallel plate inclined settler are illustrated in figure 1. Region B depicts the clear fluid layer formed underneath the downward facing surface which, under the action of buoyancy, is convected rapidly towards the top of the vessel into the clear fluid reservoir A. The interface C separates the clear fluid layer from the adjoining suspension region D, within which the particle concentration remains constant throughout the sedimentation process. In addition, since both the clear fluid and the particles are incompressible, the production of

† Present address: Molten Metal Technology, Inc., 51 Sawyer Rd, Waltham, MA 02154, USA.

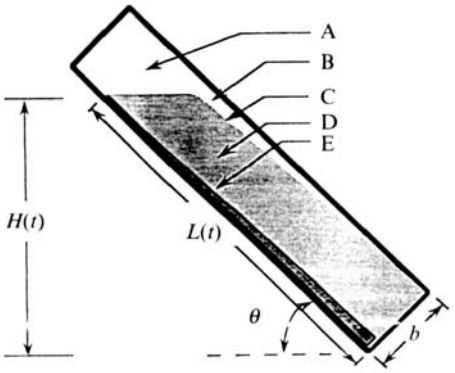

FIGURE 1. A schematic description of an inclined settler. A: clear fluid reservoir, B: clear fluid layer, C: suspension–clear fluid interface, D: suspension, E: sediment layer.

clarified fluid must be accompanied by the removal of an equivalent amount of particles from the suspension. This occurs along the upward facing surface, where a thin layer of sediment, shown as region E in figure 1, is formed which flows down the inclined plate.

A number of studies (e.g. Acrivos & Herbolzheimer 1979; Herbolzheimer & Acrivos 1981; Schneider 1982; Rubinstein 1980; Probstein, Yung & Hicks 1981; Leung & Probstein 1983; Shaqfeh & Acrivos 1986, 1987) have already examined theoretically the flow fields within the various regions of the inclined settlers and several analytic expressions for the velocity profiles within the clear fluid layer underneath the downward facing wall and within the adjoining suspension have been developed for a wide range of parameters. The formation and flow of the sediment layer on the upward facing surface was neglected, however, in most of these studies except by Probstein *et al.* (1981) and by Leung & Probstein (1983), who treated the sediment as an effective Newtonian fluid of *a priori* specified composition. But since no theory was available at that time for determining the particle concentration within the flowing concentrated sediment, such a model required the use of an adjustable parameter.

Recently, this limitation was overcome by Nir & Acrivos (1990) who, using again a continuum description, proposed a model to describe the flow of the sediment layer that forms as a result of steady sedimentation on an inclined plate. This also corresponds to the flow which develops on the upward facing surface of a 'low aspect ratio' inclined settler. The key feature of this model, which does not require any adjustable parameters, is the introduction of an equation for the particle concentration distribution involving a balance between particle convection due to the bulk flow, gravitational sedimentation, and shear-induced migration. The latter, which arises as a consequence of irreversible interparticle interactions, has been found recently to play a major role in creating the non-uniform particle concentration distributions observed experimentally in suspensions undergoing shear (Leighton & Acrivos 1986, 1987*a*, *b*; Phillips, Armstrong & Brown 1992; Koh 1991; Koh, Hookham & Leal 1994) as well as in the corresponding computer simulation studies (Brady & Bossis 1988; Durlofsky & Brady 1989). A key prediction of the model developed by Nir & Acrivos (1990) was that the particle concentration changes discontinuously across a sharp interface separating the suspension from the thin highly concentrated sediment layer. In addition, Nir & Acrivos (1990) found that the highest particle volume fraction within the sediment layer for a given angle of inclination approached the maximum possible value ϕ_m, above which the sediment is unable to flow, when the particle volume

fraction in the sedimenting suspension (ϕ_s) was either very high or very low and that the sediment layer thickness ($\tilde{\delta}$) was predicted to become very large under these conditions. But since it is natural to expect that $\tilde{\delta}$ should vanish as $\phi_s \to 0$, the theoretically predicted large values of $\tilde{\delta}$ for dilute sedimenting suspensions clearly reflects the limitations of their model.

The aim of the present paper is then to modify the model proposed by Nir & Acrivos (1990) in order to remove this anomalous prediction and test its applicability in a low aspect ratio inclined settler by means of experiments. There are of course several limitations to this model, primarily due to its use of the continuum description. In the present work, however, we shall focus our attention to two factors that may significantly affect the flow field within the flowing sediment layer and which were not considered by these investigators. First, we shall take into account the existence of an apparent slip velocity along the upward facing surface of the inclined settler arising from the fact that, in concentrated suspensions of finite-size particles flowing past a solid surface, there exists a thin film of liquid having a thickness comparable to the particle diameter within which particles may roll. As will be shown, such slip velocities at the plate can attain significant values. In addition, we shall introduce into the analysis the effect of particle migrations from regions of high shear stress to low (Leighton & Acrivos 1987*b*), which could contribute significantly to the shear-induced resuspension of particles since, according to the predictions of Nir & Acrivos (1990), large shear stress gradients can exist within the flowing sediment layer. This will be in addition to the term contributing to the particle diffusive flux due to a concentration gradient already accounted for by these investigators. As will be seen, the theoretical results for low values of the sedimenting suspension volume fraction ϕ_s are greatly affected by the introduction of these two effects, in that, as expected on physical grounds and in contrast to the result arrived at by Nir & Acrivos (1990), $\tilde{\delta}$ is now found to vanish as $\phi_s \to 0$.

The predictions based on this modified theory were tested experimentally by measuring the sediment layer thickness profile and the particle velocity profile within a sediment layer flowing in a low aspect ratio inclined settler. Such particle velocity profiles are extremely difficult to determine, in general, primarily due to the small layer thickness and the high volume fractions usually encountered within the sediment. We shall presently demonstrate, however, that this can be accomplished by first matching the refractive indices of the particles with that of the suspending fluid and then adapting the well known laser Doppler anemometry (LDA) technique to such systems. As for the sediment layer thickness, this was measured readily via a video image.

We begin by describing briefly the equations governing the motion of the flowing sediment layer together with the partial slip boundary condition at the plate and shall show that, in the limit of infinitesimally small particle Reynolds numbers, these equations are amenable to a leading-edge similarity solution. Next, we shall present the solution of these equations obtained via a finite difference scheme and shall demonstrate that, far away from the leading edge, the slip velocity at the inclined plate has a negligible effect on the flow and that a similarity solution is recovered similar to that found by Nir & Acrivos (1990). Then, in §4 we shall discuss the details of the measuring technique and of the experimental set-up that was used to perform the experiments, and, in §5, we shall show that the experimentally obtained sediment layer thicknesses and velocity profiles are in good agreement with the corresponding theoretical predictions presented in §3 in spite of the absence of any adjustable parameters in the theoretical model. Finally, we shall present in the Appendix a simple method for solving approximately the system of equations and boundary conditions developed in

§2 which, in some cases, was found to yield results in good agreement with those from the exact solution.

2. Formulation

Consider the simple two-dimensional system shown in figure 2, consisting of a surface of infinite length and arbitrary width, inclined at an angle θ to the horizontal and placed in an infinite suspension of heavy spheres of radius $\tilde{a}$. The volume fraction of particles far from the plate, also referred to as the feed particle concentration, will be denoted by ϕ_s.

The suspension is modelled as an effective Newtonian fluid with effective physical properties which, relative to the corresponding properties of the suspending liquid, are functions only of the local volume fraction of the particles. Thus, the effective density is expressed as

$$\tilde{\rho}(\phi) = \tilde{\rho}_f \gamma(\phi) \tag{1}$$

and the effective viscosity as

$$\tilde{\mu}(\phi) = \tilde{\mu}_f \lambda(\phi), \tag{2}$$

where ϕ denotes the local volume fraction of the particles, the tilde indicates that the variable in question has dimensions and the subscript f refers to the corresponding property of the clear fluid. In view of this effective continuum description, the momentum balance for a flowing suspension can therefore be written in the usual form. But, since the flowing sediment has been observed to be very thin, the standard lubrication approximation can be invoked according to which the velocity component along the inclined plate is much larger than that perpendicular to it, and also, that any variations across the sediment layer are substantially greater than those along the longitudinal direction. In addition, any changes along the normal to the (x, y)-plane shown in figure 2 are neglected. With these approximations, the x-momentum and continuity equations, when non-dimensionalized using $\tilde{a}$ and $\tilde{u}_t$ as the characteristic length and velocity scales, reduce to

$$\frac{\partial}{\partial y}\left[\lambda(\phi)\frac{\partial u}{\partial y}\right] + \tfrac{9}{2}(\phi - \phi_s)\sin\theta = R_p \gamma(\phi)\left(u\frac{\partial u}{\partial x} + v\frac{\partial u}{\partial y}\right) \tag{3}$$

and

$$\frac{\partial u}{\partial x} + \frac{\partial v}{\partial y} = 0, \tag{4}$$

where $\tilde{u}_t = \frac{2}{9}\tilde{a}^2(\tilde{\rho}_s - \tilde{\rho}_f)/\tilde{\mu}_f$ is the Stokes settling speed in the clear fluid of a single sphere of density $\tilde{\rho}_s$ and $R_p = \tilde{\rho}_f \tilde{u}_t \tilde{a}/\tilde{\mu}_f$ is the particle Reynolds number based on the relative motion between the particles and the fluid. Since R_p is typically very small in most systems of practical interest, the right-hand-side term in equation (3) will henceforth be neglected within the sediment layer. In addition, as can be shown easily by applying the momentum balance in the y-direction, the pressure drop across the thin sediment layer is negligible to this order of approximation.†

As mentioned earlier, the presence of shear in a concentrated suspension induces a migration of particles within the suspension which, along with the sedimentation flux

† Strictly speaking, the continuity equation as given by (4) is incorrect because it does not account for changes in the density of the suspension that result from variations in ϕ within the sediment layer. It can easily be shown, however, from the work to be presented later in this paper that, for the system tested experimentally, the change in the relative density across the sediment layer never exceeded about 10%, hence the simplified form of the continuity equation given above will be retained throughout the analysis.

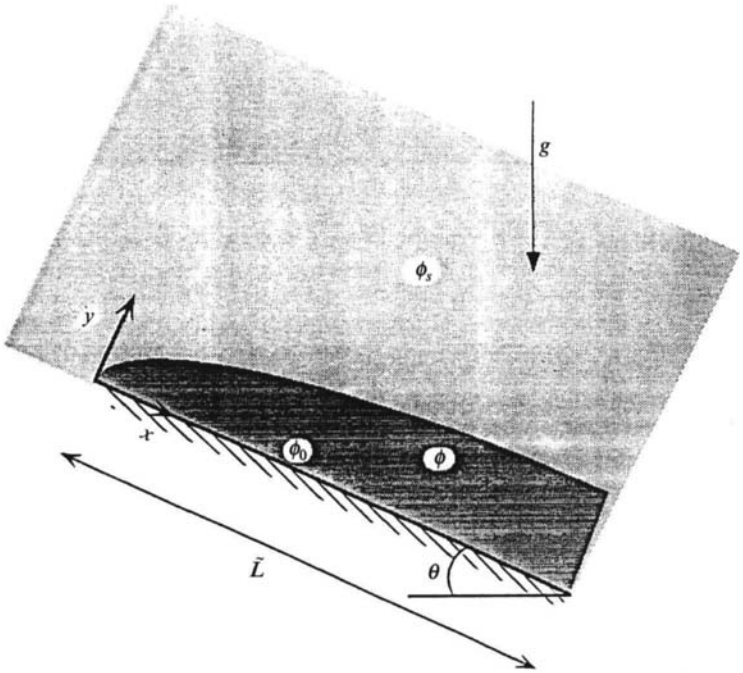

FIGURE 2. A schematic description of sediment flow on an inclined plane.

and the bulk flow, leads to a non-uniform particle concentration, ϕ. To determine this profile, however, it is necessary to examine, in addition to the momentum equation, the equation for the steady-state particle balance

$$u\frac{\partial\phi}{\partial x}+v\frac{\partial\phi}{\partial y}+\frac{\partial}{\partial y}(N_g)+\frac{\partial}{\partial y}(N_d)=0, \tag{5}$$

where N_g and N_d denote, respectively, the dimensionless flux of particles due to gravity settling and that due to shear-induced diffusion in the y-direction. For the case of a monodispersed suspension of spheres, the former can be expressed as

$$N_g=-\phi f(\phi)\cos\theta, \tag{6}$$

where $f(\phi)$ is the so-called hindrance function which accounts for the effects of the other particles on the sedimentation velocity. Once again, in view of the lubrication approximation, the flow can be treated as quasi-unidirectional with the term $\partial u/\partial y$ becoming the dominant component in the velocity gradient tensor. Thus, following the work of Leighton & Acrivos (1987*b*), the diffusive flux which accounts for shear-induced diffusion due to concentration as well as shear stress gradients can be expressed in terms of the dimensionless variables introduced earlier as

$$N_d=-\left[\beta(\phi)\left|\frac{\partial u}{\partial y}\right|\frac{\partial\phi}{\partial y}+\frac{\alpha(\phi)}{\lambda(\phi)}\frac{\partial}{\partial y}\left(\lambda(\phi)\left|\frac{\partial u}{\partial y}\right|\right)\right], \tag{7}$$

where α and β are functions only of ϕ whose explicit form, taken in the present analysis, will be discussed in §3.

The appropriate boundary conditions at $y = 0$ are

$$v = 0 \tag{8}$$

and

$$\left[\beta(\phi)\frac{\partial u}{\partial y}\frac{\partial \phi}{\partial y} + \frac{\alpha(\phi)}{\lambda(\phi)}\frac{\partial}{\partial y}\left(\lambda(\phi)\frac{\partial u}{\partial y}\right)\right] + \phi f(\phi)\cos\theta = 0, \tag{9}$$

where the latter reflects the fact that the settling flux of the particles must be balanced by a corresponding shear-induced diffusive flux if the net particle flux into the wall is to vanish. Thus, according to this model, the existence of the shear-induced particle diffusion prevents the concentration of particles at the wall from reaching its maximum value where the suspension viscosity become infinite and thereby plays a crucial role in maintaining the flow of the sediment layer.

These equations were first analysed by Nir & Acrivos (1990) for the case $\alpha \equiv 0$, i.e. in the absence of shear-induced diffusion due to gradients in the shear stress, subject to the additional boundary condition of no slip, i.e. $u = 0$ at $y = 0$. As was pointed out by these investigators, the boundary layer along the inclined plate can be viewed as consisting of two overlapping sublayers. Specifically, in the region adjacent to the inclined plate, termed the viscous sublayer, the viscous forces in equation (3) balance the force due to buoyancy, and the inertia terms are negligible to leading order. Beyond this viscous sublayer, however, the particle concentration essentially equals ϕ_s and, therefore, the inertial terms must be retained in equation (3). In addition, these investigators showed that the particle concentration must undergo a jump across a sharp interface separating these sublayers and that the entire variation of the particle volume fraction is confined within the viscous sublayer of finite thickness, $\hat{\delta} \equiv \tilde{\delta}/\tilde{a}$, termed the sediment layer, beyond which the buoyancy term in equation (3) vanishes identically.

Unlike the previous work of Nir & Acrivos (1990), the present analysis will examine the consequences of having both a slip velocity at the inclined plate as well as $\alpha \neq 0$. But since neither of these modifications alters the structure of the governing equations, we would expect the gross features of the solution to remain unchanged. Thus we shall restrict our attention to the sediment layer mentioned above.

We begin by replacing the no-slip boundary condition with

$$u = \zeta(\partial u/\partial y)_{y=0} \quad \text{at} \quad y = 0, \tag{10}$$

where ζ is the slip coefficient, rendered dimensionless with $\tilde{a}$, which in general will depend on the microstructure of the suspension close to the wall; however, to a first approximation ζ will be taken to be a function only of the particle volume fraction at the wall. As was mentioned in the introduction, the existence of an effective slip velocity is due to the fact that, since the particles are of finite size, the continuum approximation fails within $O(\tilde{a})$ distance from the wall. In addition, we note that since the strain rate at the wall is $O(u_b/\hat{\delta})$, where u_b is a measure of the bulk velocity within the sediment layer, the slip velocity at the wall relative to u_b is $O(\zeta/\hat{\delta})$ on account of (10). Therefore, in view of the fact that $\hat{\delta}$ is a monotonically increasing function of x, we would expect the influence of the slip velocity to become progressively weaker far from the leading edge of the sediment layer and that the boundary condition (10) will reduce to the no-slip condition $u = 0$. Clearly, the domain of x within which partial slip at the plate may have a significant effect on the solution will depend strongly on the magnitude of the slip coefficient ζ.

Without loss of generality, let us then consider the region of x within which partial slip at the wall is important. First of all, on balancing the first and last terms of (5) with

N_d given by (7), we find on account also of (3) – with its right-hand-side term set equal to zero – and (10), that $\zeta_c \hat{\delta}^2/x \sim O(1)$ and $u = O(\zeta_c \hat{\delta})$, thereby implying that $v = O(1)$ from continuity, where ζ_c denotes a value of the dimensionless slip coefficient characteristic of the particular problem being considered. Accordingly, $\hat{\delta}/\zeta_c \sim O(x/\zeta_c^3)^{1/2}$ and $u/\zeta_c^2 \sim O(x/\zeta_c^3)^{1/2}$, which in turn, lead to the transformations

$$Y = y/\zeta_c, \quad X = x/\zeta_c^3, \quad U = u/\zeta_c^2 \quad \text{and} \quad V = v. \tag{11}$$

In terms of these new variables, the system of equations then becomes

$$\frac{\partial}{\partial Y}\left[\lambda(\phi)\frac{\partial U}{\partial Y}\right] + \tfrac{9}{2}(\phi - \phi_s)\sin\theta = O(R_p\,\zeta_c), \quad \frac{\partial U}{\partial X} + \frac{\partial V}{\partial Y} = 0 \tag{12}$$

and

$$U\frac{\partial \phi}{\partial X} + V\frac{\partial \phi}{\partial Y} - \cos\theta\frac{\partial \phi}{\partial Y}\frac{d}{d\phi}[\phi f(\phi)] = \beta(\phi)\frac{\partial U}{\partial Y}\frac{\partial^2 \phi}{\partial Y^2} + \frac{\partial \phi}{\partial Y}\left[\lambda(\phi)\frac{\partial U}{\partial Y}\frac{\partial \phi}{\partial Y}\frac{d}{d\phi}\left(\frac{\beta(\phi)}{\lambda(\phi)}\right)\right.$$
$$\left. - \tfrac{9}{2}\sin\theta\left\{\frac{\beta(\phi)}{\lambda(\phi)}(\phi - \phi_s) + \frac{d}{d\phi}\left(\frac{\alpha(\phi)}{\lambda(\phi)}(\phi - \phi_s)\right)\right\}\right], \tag{13}$$

where, in arriving at (13) from (5), use has been made of (6), (7) and (12). In addition, the boundary conditions of partial slip, impermeability and zero particle flux at the wall, $Y = 0$, become

$$U = q(\partial U/\partial Y)_{Y=0}, \quad V = 0 \tag{14}$$

and

$$\left[\beta(\phi)\frac{\partial U}{\partial Y}\frac{\partial \phi}{\partial Y} + \frac{\alpha(\phi)}{\lambda(\phi)}\frac{\partial}{\partial Y}\left(\lambda(\phi)\frac{\partial U}{\partial Y}\right)\right] + \phi f(\phi)\cos\theta = 0, \tag{15}$$

where $q = \zeta/\zeta_c$, which in general would be an $O(1)$ quantity if ζ_c is chosen properly.

In order to complete the mathematical formulation of the problem, however, it is necessary to specify the remaining boundary conditions at the sediment–suspension interface. As pointed out earlier, within the sediment layer the viscous term in (3) balances the force due to buoyancy and inertia effects are negligible to the first order while, within the suspension region, the particle concentration is asymptotically equal to ϕ_s and the inertial term in (3) must be retained. Now, given that U – which on account of the relation preceding (11) is $O(X^{1/2})$ – must remain continuous across the sediment–suspension interface, it is easy to show that the ratio of the sediment layer thickness, $O(X^{1/2})$, to that of the inertial layer is $O(\zeta_c^{1/2} R_p^{1/2} X^{1/4})$. Hence, in view of the requirement that the shear stress also be continuous across this interface, it follows that, as the edge of the viscous layer is approached from below,

$$\frac{\partial U}{\partial Y} = \frac{\lambda(\phi_s)}{\lambda(\phi_\delta)} O(\zeta_c R_p X^{1/2})^{1/2} \to 0 \quad \text{for} \quad R_p \to 0, \tag{16}$$

where ϕ_δ refers to the corresponding particle volume fraction within the sediment along this interface. Consequently, the longitudinal velocity component would be expected to increase monotonically from the wall to its maximum value at the edge of the sediment layer.

It was also reported by Nir & Acrivos (1990) that the set of equations which apply within the viscous sublayer do not have a solution if the particle volume fraction is set equal to ϕ_s at the edge of this layer. These investigators were led to conclude therefore that the particle concentration ϕ must suffer a jump across the interface separating the concentrated sediment from the bulk of the suspension and that the entire variation in ϕ must be primarily confined within a viscous layer of finite thickness. One condition

which clearly must be satisfied at this interface is that the particle flux be continuous across it. Hence, if, in the transformed coordinates of (11), the edge of the viscous sublayer is denoted by $Y = \delta(X) \equiv \hat{\delta}/\zeta_c \equiv \tilde{\delta}/\tilde{a}\zeta_c$, this becomes

$$\left[-U_\delta\frac{\mathrm{d}\delta}{\mathrm{d}X}+V_\delta-f(\phi_\delta)\cos\theta\right]\phi_\delta+\frac{9\alpha(\phi_\delta)}{2\lambda(\phi_\delta)}(\phi_\delta-\phi_s)\sin\theta=\left[-U_\delta\frac{\mathrm{d}\delta}{\mathrm{d}X}+V_\delta-f(\phi_\delta)\cos\theta\right]\phi_s, \tag{17}$$

where ϕ_δ denotes the particle concentration as the interface is approached from below and U_δ and V_δ are the corresponding velocity components evaluated at $Y = \delta(X)$. Although (17) is obviously satisfied when $\phi_\delta = \phi_s$, the governing equations within the viscous layer subject to this boundary condition do not have a solution for any choice of δ and therefore some additional physical information or another boundary condition is needed if both ϕ_δ and $\delta(X)$ are to be determined. This is provided by the fact that (13) becomes singular at the edge of the viscous layer since $(\partial U/\partial Y)$, which is also proportional to the coefficient of the highest derivative in that equation, vanishes as $Y \to \delta(X)$ in view of (16). Hence, following Nir & Acrivos (1990), it suffices to require that ϕ be regular for $Y \leqslant \delta(X)$ or, more generally, that

$$\lim_{Y\to\delta(X)}\left(\frac{\partial U}{\partial Y}\frac{\partial^2\phi}{\partial Y^2}\right)=0 \tag{18}$$

which when substituted into (13) leads to

$$U_\delta\frac{\mathrm{d}\phi_\delta}{\partial X}+\left(\frac{\partial\phi}{\partial Y}\right)_{Y=\delta}\left\{-U_\delta\frac{\mathrm{d}\delta}{\mathrm{d}X}+V_\delta-\frac{\mathrm{d}}{\mathrm{d}\phi_\delta}\left(\phi_\delta f(\phi_\delta)\cos\theta-\frac{9\alpha(\phi_\delta)}{2\lambda(\phi_\delta)}(\phi_\delta-\phi_s)\sin\theta\right)\right.$$
$$\left.+\frac{9\beta(\phi_\delta)}{2\lambda(\phi_\delta)}(\phi_\delta-\phi_s)\sin\theta\right\}=0 \tag{19}$$

when the terms containing $\partial U/\partial Y$ are set equal to zero. In view of the flux matching condition across the interface, equation (17), the above equation can be rewritten as

$$U_\delta\frac{\mathrm{d}\phi_\delta}{\mathrm{d}X}+\left(\frac{\partial\phi}{\partial Y}\right)_{Y=\delta}\mathscr{F}(\phi_\delta,\phi_s,\theta)=0 \tag{20}$$

with

$$\mathscr{F}(\phi_\delta,\phi_s,\theta)=-\frac{9}{2\lambda(\phi_\delta)}(\phi_\delta-\phi_s)\left(-\beta(\phi_\delta)+\frac{\alpha(\phi_\delta)}{(\phi_\delta-\phi_s)}\right)\sin\theta+\frac{(\phi_\delta f(\phi_\delta)-\phi_s f(\phi_s))}{(\phi_\delta-\phi_s)}\cos\theta$$
$$-\frac{\mathrm{d}}{\mathrm{d}\phi_\delta}\left(\phi_\delta f(\phi_\delta)\cos\theta-\frac{9\alpha(\phi_\delta)}{2\lambda(\phi_\delta)}(\phi_\delta-\phi_s)\sin\theta\right) \tag{21}$$

which appears to be a part of a system of coupled set of PDEs plus boundary conditions that need to be solved numerically before the jump across the interface $(\phi_\delta-\phi_s)$ could be determined. In the limit of large X, i.e. in the absence of slip at the wall, however, it was shown by Nir & Acrivos (1990) that the particle concentration ϕ within the sediment layer attains a self-similar profile, which in turn reduces the differential equation (20) to a simple nonlinear algebraic equation

$$\mathscr{F}(\phi_\delta,\phi_s,\theta)=0 \tag{22}$$

with the only unknown being ϕ_δ, since the derivative of ϕ_δ with respect to X vanishes for this case. In fact, as will be shown later in §2.1, the condition $\mathrm{d}\phi_\delta/\mathrm{d}X = 0$ turns out

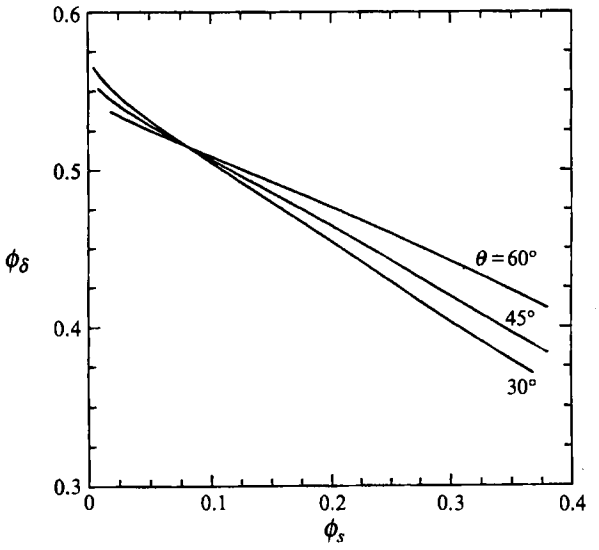

FIGURE 3. Theoretically predicted particle volume fraction at the edge of the sediment layer, ϕ_δ, as a function of ϕ_s, for $\theta = 30°$, 45° and 60°.

to be the only possibility consistent with the system of equations and boundary conditions given above. Thus, the jump in concentration $(\phi_\delta - \phi_s)$ can be determined from (21) and (22) once and for all, given the values of ϕ_s and θ. Figure 3 shows a typical solution of this jump condition for the particular choice of the functions λ, α, β and f reported in §3, cf. (42)–(45).

The governing equations (12) and (13) along with the boundary conditions (14), (15), (16), (17) and (22) form then a complete set of partial differential equations, which is valid within the viscous sublayer for the entire range of X provided that the particle Reynolds number R_p is sufficiently small for (16) to apply. Although, in general, this set needs to be solved numerically, it will be seen presently that the system admits a similarity solution for $X \ll 1$ in addition to the similarity solution found by Nir & Acrivos (1990) for $X \gg 1$.

2.1. *Analysis with partial slip (small-X solution)*

Since equations (12) and (13) are identical to those studied by Nir & Acrivos (1990) for the case of no slip, except for one extra term in (13) which accounts for the shear-induced migration of particles due to shear stress gradients, the solutions of the two sets would be expected to have many features in common. However, on account of the partial slip boundary condition (10), the similarity solution derived by Nir & Acrivos (1990) no longer applies. Nevertheless, a closer examination of (12) and (13) suggests that these equations along with the boundary conditions are amenable to a leading-edge expansion

$$\left.\begin{aligned} U &= AX^{1/2}\cos\theta + F'(\eta)\,X\cos\theta + O(X^{3/2}), \\ \phi &= \phi(\eta) + O(X^{1/2}), \end{aligned}\right\} \tag{23}$$

with $\eta = Y/X^{1/2}$. Then, on substituting the above plus the expression for V, as obtained from the continuity equation, into the momentum and mass balance equations, one obtains, with the primes indicating differentiation with respect to η,

$$(\lambda(\phi)\,G(\eta))' + \tfrac{9}{2}(\phi - \phi_s)\tan\theta = 0 \tag{24}$$

and

$$(\beta(\phi)\,G(\eta)\,\phi')' - \left(\frac{9\alpha(\phi)}{2\lambda(\phi)}(\phi-\phi_s)\tan\theta\right)' + \phi'\left[A\eta + \frac{\mathrm{d}}{\mathrm{d}\phi}(\phi f(\phi))\right] = 0, \tag{25}$$

where $G = F''$, subject to the boundary conditions along the inclined plate at $\eta = 0$

$$A = G(0) \quad \text{(slip condition)} \tag{26}$$

and

$$\beta(\phi_0)\,G(0)\,\phi'|_{\eta=0} - \frac{9\alpha(\phi_0)}{2\lambda(\phi_0)}(\phi_0-\phi_s)\tan\theta + \phi_0 f(\phi_0) = 0 \quad \text{(no-flux condition)}, \tag{27}$$

where ϕ_0 denotes the unknown particle volume fraction adjacent to the surface of the inclined plate. It should be noted that, in arriving at (26) from (14), q has been taken as unity by choosing $\zeta_c = \zeta(\phi_0)$.

As mentioned earlier, the longitudinal velocity attains its maximum value at the sediment–suspension interface, i.e. at the edge of the viscous layer of thickness $\delta(X) = \delta_0 X^{1/2}$. Therefore,

$$G(\delta_0) = 0 \quad \text{at} \quad \eta = \delta_0. \tag{28}$$

Also, the flux of particles leaving the suspension should equal the particle flux entering the sediment layer, which requires that the total flux of particles across the curve $Y = \delta(X) = \delta_0 X^{1/2}$ should remain the same on either side of the suspension–sediment interface. Thus, if once again the particle volume fraction in the sediment layer just below $\eta = \delta_0$ is denoted by ϕ_δ, which is known on account of (21) and (22), the flux matching condition at $\eta = \delta_0$ becomes

$$(A\delta_0 + f(\phi_s))\,\phi_s = (A\delta_0 + f(\phi_\delta))\,\phi_\delta - \frac{9\alpha(\phi_\delta)}{2\lambda(\phi_\delta)}(\phi_\delta-\phi_s)\tan\theta, \tag{29}$$

which is clearly a special form of the general expression (17) derived earlier. Thus, for given values of ϕ_s, θ and ϕ_δ, the above expression determines $A\delta_0$.

It is appropriate at this point to examine the validity of (22), i.e. the solution proposed earlier for (20). Suppose that $\mathscr{F} \neq 0$. But, in view of the expansion (23) in the limit as $X \to 0$, the longitudinal velocity and the transverse coordinate within the sediment layer scale as $U \sim X^{1/2}$ and $Y \sim X^{1/2}$, respectively, which in turn yields

$$X\,\mathrm{d}\phi_\delta/\mathrm{d}X = O(1) \tag{30}$$

from (20) since $\mathscr{F}$ is independent of X as the leading edge is approached. Clearly then since, according to the above expression, the first-order correction to ϕ_δ should be $O(\ln X)$ which does not vanish as $X \to 0$, the only possibility for small X, and in fact for any X in view of the parabolic nature of the governing equations, is (22).

The system of equations and boundary conditions thus obtained can be recast into a boundary value problem consisting of a single third-order ordinary differential equation plus one unknown parameter, A or δ_0, and four boundary conditions. The latter are (26), (27), (28) together with the known values of $\phi = \phi_\delta$ at $\eta = \delta_0$ and $A\delta_0$. This system can be further simplified, however, by introducing the transformations

$$\xi = \eta/\delta_0 \quad \text{and} \quad g = G/\delta_0 \tag{31}$$

in terms of which the governing equations are as before except for the fact that the unknown parameter A in (25) has been replaced with the known term $A\delta_0$. Thus, with this change of notation, (24) and (25), subject to the boundary conditions (27) and (28) plus the known value of ϕ_δ at $\xi = 1$, reduce to a simple third-order boundary value

problem within the domain of integration $0 \leqslant \xi \leqslant 1$. Once such a solution is obtained, the sediment layer thickness parameter δ_0 can then be easily determined from the slip boundary condition (26) which becomes

$$\delta_0 = (A\delta_0/g(0))^{1/2} \tag{32}$$

in terms of the already known parameter $A\delta_0$ and the values of $g(0)$ and ϕ_0 as computed from the numerical integration. Furthermore, if we defined the sediment layer thickness relative to the particle radius as $\hat{\delta}(x) = \hat{\delta}_0 x^{1/2}$, then, following the transformations given by (11), we obtain

$$\hat{\delta}_0 = \delta_0/\zeta_c^{1/2} \quad \text{with} \quad \zeta_c \equiv \zeta(\phi_0) \tag{33}$$

which in turn can be used to obtain the sediment layer thickness relative to the particle size at any point x radii beyond the leading edge provided that $X \ll 1$.

It should be noted here that the solution referred to above only yields the leading-order terms of the velocity and particle concentration expansions, which coincide with the exact solution only as X approaches zero.

2.2. *Analysis with no-slip (large-X solution)*

As discussed earlier, following (10), the slip boundary condition (10) or (14) reduces far away from the leading edge to

$$U = 0 \quad \text{at} \quad Y = 0 \quad \text{for} \quad X \to \infty \tag{34}$$

since δ increases monotonically with X. Consequently, on balancing the convection and diffusive terms in (13) and noting that, now, $\partial U/\partial Y \sim O(U/\delta)$, we conclude that $\delta \sim X^{1/3}$. On the other hand, on neglecting the inertia terms in (12) we find that $U \sim O(\delta^2) = O(X^{2/3})$. Therefore, as shown already by Nir & Acrivos (1990) for the special case $\alpha \equiv 0$, the governing equations (12) and (13), along with the boundary conditions equations (14), (15), (16) and (17), are amenable to a similarity solution of the type

$$U = X^{2/3} F'(\eta) \cos\theta, \quad \phi = \phi(\eta), \tag{35}$$

with $\eta = Y/X^{1/3}$ and, as before, with the prime denoting differentiation with respect to η. In view of this transformations, the governing equations reduce to

$$(\lambda(\phi) F''(\eta))' + \tfrac{9}{2}(\phi - \phi_s)\tan\theta = 0 \tag{36}$$

and

$$(\beta(\phi) F''(\eta)\phi')' - \left(\frac{9\alpha(\phi)}{2\lambda(\phi)}(\phi - \phi_s)\tan\theta\right)' + \phi'\left[F + \frac{\mathrm{d}}{\mathrm{d}\phi}(\phi f(\phi))\right] = 0 \tag{37}$$

subject to the boundary conditions at the inclined plate,

$$F = F' = 0 \quad \text{at} \quad \eta = 0 \tag{38}$$

and

$$\beta(\phi_0) F''(0)\phi'|_{\eta=0} - \frac{9\alpha(\phi_0)}{2\lambda(\phi_0)}(\phi_0 - \phi_s)\tan\theta + \phi_0 f(\phi_0) = 0 \quad \text{(no-flux condition)}, \tag{39}$$

where ϕ_0 refers as before to the unknown particle volume fraction next to the plate. On the other hand, the boundary conditions at the sediment–suspension interface $Y = \delta(X) = \delta_\infty X^{1/3}$ now reduce to

$$F'' = 0 \tag{40}$$

and

$$(F_\delta + f(\phi_s))\phi_s = (F_\delta + f(\phi_\delta))\phi_\delta - \frac{9\alpha(\phi_\delta)}{2\lambda(\phi_\delta)}(\phi_\delta - \phi_s)\tan\theta, \tag{41}$$

where the latter, reflecting the continuity of particle flux across the interface $\eta = \delta_\infty$, is a special form of the general expression (17) derived earlier. Equation (41) serves then as the boundary condition for F at $\eta = \delta_\infty$ since the particle concentration ϕ_s is already known at this point from the solution of (22), for given values of ϕ_s and θ.

In contrast to the case with partial slip described earlier, these equations require the solution of a fifth-order boundary value problem together with a one-parameter search which arises because the sediment layer thickness δ_∞, and therefore the domain of integration $(0, \delta_\infty)$, is not known *a priori*. It is also worth remarking that, in view of (11) and (35), both $\hat{\delta}(X)$, the sediment layer thickness relative to the particle radius $\tilde{a}$, as well as the two velocity components U and V are independent of ζ_c as $X \to \infty$ which, of course, is as it should be. Consequently, far from the leading edge, $\hat{\delta}(X) \to \delta_\infty x^{1/3}$ where δ_∞ is obtained as part of the numerical solution of the similarity equations given above.

3. Theoretical predictions

In order to solve the nonlinear set of ordinary differential equations described earlier in §2, explicit forms for the functions α, β, λ and f are needed. Following Leighton & Acrivos (1986, 1987*b*), these will be chosen as

$$\lambda(\phi) = \left(1 + \frac{1.5\phi}{1-\phi/\phi_m}\right)^2, \tag{42}$$

$$\alpha(\phi) = K_\sigma \phi^2, \tag{43}$$

and

$$\beta(\phi) = \tfrac{1}{3}\phi^2(1 + \tfrac{1}{2}e^{8.8\phi}), \tag{44}$$

where ϕ_m, taken here as 0.58, denotes the maximum possible concentration of the particles in a flowing suspension and K_σ is an order-one weak function of ϕ. Owing to the lack of experimental data for the system considered here, calculations were performed for $K_\sigma = 0.6$, which is close to the value of K_σ obtained experimentally by Leighton & Acrivos (1987*b*) for a channel flow. Moreover, since the hindrance function f appropriate to this problem is unavailable in the literature, the settling velocity of a sphere in the suspension undergoing shear will be set equal to its Stokes settling velocity in a fluid with viscosity $\mu(\phi)$ and density $\rho(\phi)$, thereby leading to the expression for the hindrance function

$$f(\phi) = (1-\phi)/\lambda(\phi) \tag{45}$$

which, in view of (42), vanishes as $\phi \to \phi_m$. This expression for f has also been used by Leighton & Acrivos (1986) and by Schaflinger, Acrivos & Zhang (1990). Unlike the functions described above, however, very little information is available in the literature regarding the dependence of ζ on ϕ_0. Nevertheless, it can be easily shown (Kapoor 1994) that a simple expression for ζ can be obtained for concentrated suspensions by making use of an effective continuum model due to Acrivos & Chang (1986) and Chang & Acrivos (1987) which leads to the prediction that ζ should be proportional to $[\lambda(\phi_0) - 1]$. This prediction was tested by means of an independent set of experiments in a Couette device (Jana, Kapoor & Acrivos 1995), and the data thereby obtained were found to follow the expression

$$\zeta = \tfrac{1}{8}[\lambda(\phi_0) - 1] \approx \tfrac{1}{8}\lambda(\phi_0) \tag{46}$$

for $0.45 \leqslant \phi_0 \leqslant 0.52$.

Given these choices for the various functions described above, the system of equations discussed in §§2.1 and 2.2 were solved first. Figure 3 depicts the solution of

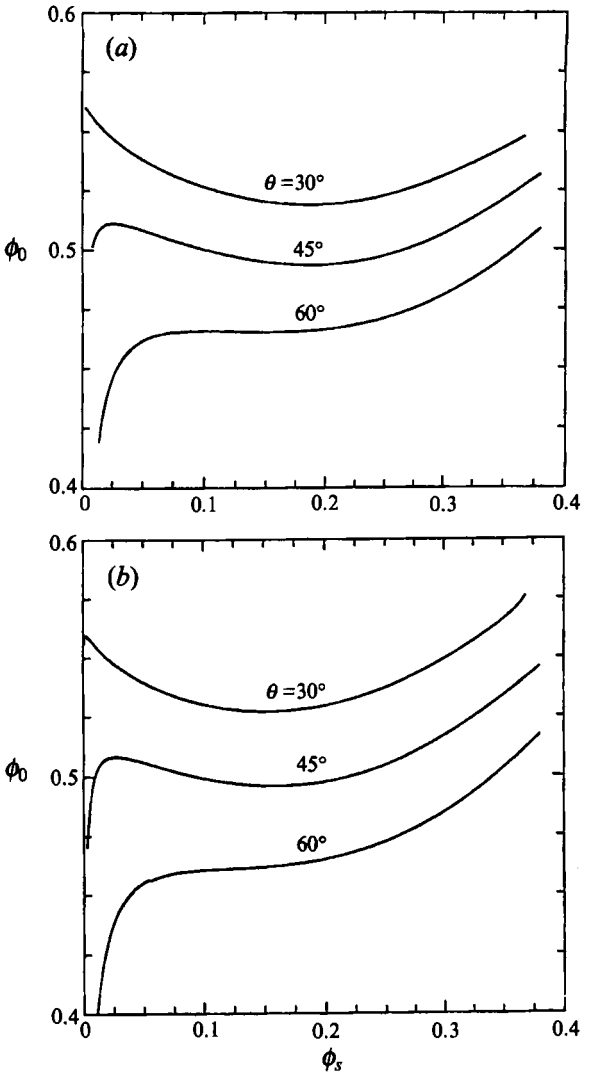

FIGURE 4. The particle volume fraction at the plate, ϕ_0, as a function of ϕ_s, for $\theta = 30°$, 45° and 60°: (*a*) the small-X asymptotic solution; (*b*) the large-X asymptotic solution.

the jump condition (22) as a function of the feed particle concentration ϕ_s, for various angles of inclinations. Because (22) does not involve X, the change in the particle volume fraction across the interface $(\delta_s - \phi_s)$ is the same over the entire range of X under identical conditions. As discussed earlier, the value of ϕ_δ thus obtained is then used as a boundary condition along with (26), (27) and (28) to construct a solution to the governing equations (24) and (25) which apply for $X \ll 1$. The particle volume fraction at the plate, ϕ_0, thereby computed is shown in figure 4(*a*) as a function of ϕ_s for various angles of inclinations. The decrease in ϕ_0 as θ increases merely reflects the increase in the diffusive flux of the particles due to the higher shear rates. As shown in figure 4(*b*), the corresponding solutions for large X also show a similar behaviour. On comparing figures 4(*a*) and 4(*b*) with the corresponding predictions for ϕ_δ shown in figure 3, it is apparent that for small angles of inclination and for intermediate to small values of ϕ_s, the variations of the particle volume fraction ϕ within the sediment layer

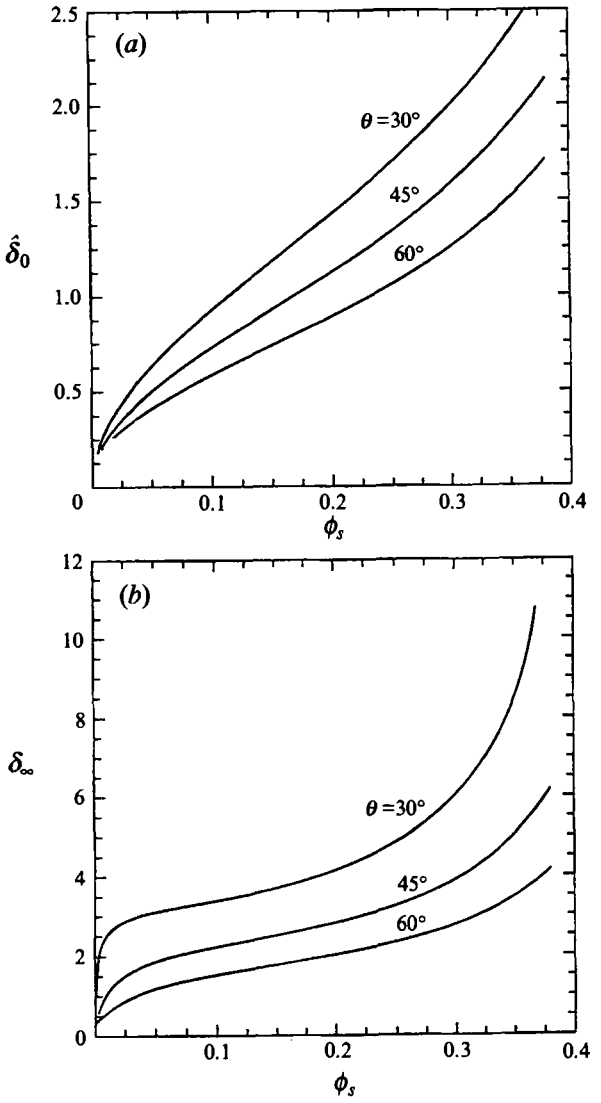

FIGURE 5. The sediment layer thickness parameter, as a function of ϕ_s, for $\theta = 30°$, 45° and 60°: (*a*) $\hat{\delta}_0$, for the small-X solution; (*b*) δ_∞, for the large-X solution.

are negligibly small. Thus, under these conditions the particle volume fraction ϕ can be assumed to be uniform within the entire sediment layer and approximately equal to ϕ_s. In that case, the particle balance equation within the sediment layer given by (13) can be discarded and approximate but accurate expressions for the sediment layer thickness and for the corresponding velocity profile can be obtained for all values of X, as shown in the Appendix.

Once (24) and (25) have been solved, $\zeta_c(\phi_0)$ can be calculated from (42) and (46) and the sediment layer thickness parameter $\hat{\delta}_0$ can be easily evaluated from (32) and (33). Shown in figure 5(*a*) is the effect of a change in the angle of inclination on $\hat{\delta}_0$ as a function of the feed particle concentration, while the variation of the corresponding thickness parameter δ_∞ for the large-X solution is shown in figure 5(*b*). On comparing these two figures with that for the case of no slip and with $\alpha = 0$ (Nir & Acrivos 1990),

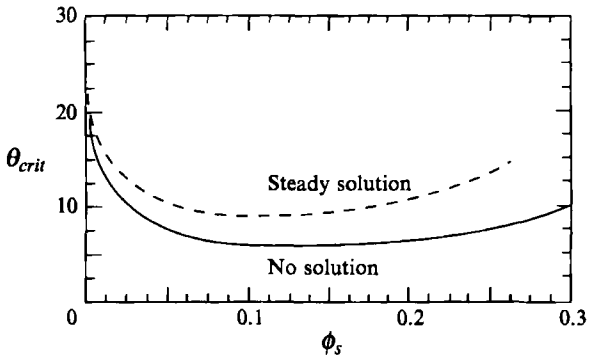

FIGURE 6. The critical angle of inclination below which a steady motion of the sediment layer cannot exist, as a function of ϕ_s: ——, theory with slip; – – –, theory without slip.

it is seen that the inclusion of slip as well as diffusion due to gradients in the shear stress alters the qualitative nature of the sediment layer thickness profile in a major way, and that the puzzling result reported by Nir & Acrivos (1990) for $\alpha = 0$, in which δ_∞ was found to increase without bound as $\phi_s \to 0$, is thereby eliminated.

According to the effective continuum model adopted here, there exist two possible mechanisms by which the sediment layer thickness can approach zero in the limit $\phi_s \to 0$. The first possibility occurs when the average concentration within the sediment layer remains close to ϕ_m and the slip velocity at the inclined plate is an $O(1)$ quantity. Physically this represents a plug of constant concentration slipping along the inclined plate. The second possibility is when the particle concentration close to the wall remains less than its average value within the sediment layer. But if the boundary condition (27) is examined closely, it becomes clear that, in the absence of shear-induced diffusion due to a gradient in the shear stress, the particle volume fraction will always increase monotonically away from the wall to balance the gravitational particle flux. Therefore, within the framework of the model proposed by Nir & Acrivos (1990), resuspension due to a concentration gradient alone subject to the no-slip boundary condition at the wall can never lead to a sediment layer thickness which approaches zero as $\phi_s \to 0$. However, when $\alpha \neq 0$ the contribution due to the shear stress gradient term enhances the resuspension process which in turn reduces the average particle concentration within the sediment and leads to a relatively thinner sediment layer. In fact, for higher values of α, the gravitational flux and the diffusion flux due to a concentration gradient will act in the same direction in order to balance the diffusive flux due to the shear stress gradient.

Figure 6 shows the domain within which a steady-state solution of the boundary layer equations will exist for the small-X and the large-X asymptotic solutions respectively, with the solid line indicating the location of the boundary for the small-X asymptotic solution at which ϕ_0, the particle concentration at the plate, reaches ϕ_m and the sediment ceases to flow, while the dashed line refers to the corresponding predictions from the large-X asymptotic solution.

The theoretical predictions presented above describe the flowing sediment layer either near the leading edge of the inclined plate or far downstream. But, in order to draw a meaningful comparison with the experiments and also to determine the range of applicability of these asymptotic solutions, it is necessary to obtain a complete numerical solution valid for all X. Clearly, the momentum and particle balance equations (12) and (13) along with the continuity equation are parabolic with X as a

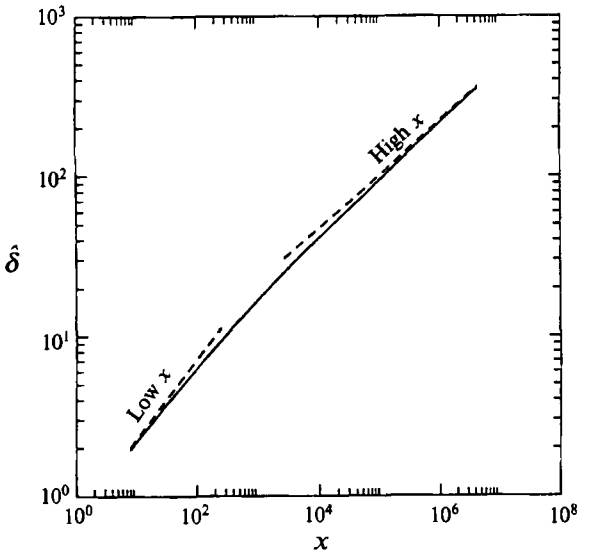

FIGURE 7. The theoretically predicted sediment layer thickness $\hat{\delta}$ as a function of the distance x from the leading edge, both rendered dimensionless with the particle radius $\bar{a}$, together with the corresponding asymptotic expression for small x and for large x, for $\phi_s = 9.6\%$ and $\theta = 45°$.

marching coordinate and can be solved by a number of numerical techniques. Here we chose the method of finite differences and began the integration at some small X where the leading-edge solution provided the appropriate initial condition. In addition, the parameter ζ_c was taken as the value of $\zeta(\phi_0)$ from the small-X asymptotic solution. The specific details of the numerical technique employed are given elsewhere (Kapoor 1994). A typical result of the numerical solution is shown in figure 7, which depicts the variation with x of the dimensionless sediment layer thickness $\hat{\delta}$, for $\phi_s = 9.6\%$ and $\theta = 45°$. The dashed lines in this figure refer to the asymptotic solutions at low as well as high X based on the analysis presented earlier in §§2.1 and 2.2. Clearly, the numerical computed sediment layer thickness profile $\hat{\delta}(x)$ is consistent with the results of the asymptotic analysis, and can be approximated by the simple interpolation formula

$$\frac{\hat{\delta}_0 x^{1/2}}{\hat{\delta}} = \left[1 + \left(\frac{\hat{\delta}_0 x^{1/2}}{\hat{\delta}_\infty x^{1/3}}\right)^{5/2}\right]^{2/5}, \tag{47}$$

where the thickness parameters $\hat{\delta}_0$ and $\hat{\delta}_\infty$ introduced earlier are the coefficients of the asymptotic expressions $\hat{\delta} = \hat{\delta}_0 x^{1/2}$ and $\hat{\delta} = \hat{\delta}_\infty x^{1/3}$ as $X \to 0$ and $X \to \infty$, respectively. Together with the graphs presented in figures 5(*a*) and 5(*b*), this interpolation formula can be readily used to compute the sediment layer thickness $\hat{\delta}$ for intermediate ranges of x.

4. Experimental investigation

The complete characterization of the sediment layer requires the determination of its thickness profile, the particle velocity profile, and the corresponding particle concentration profile. The former is relatively easy to measure experimentally by means of a cathetometer or by employing a video imaging technique. Although, in principle, both methods require that a good optical contrast should exist between the

suspension and the sediment, in all cases the sediment layer thickness could be measured manually from a video image to within ~ 0.03 mm even though, as discussed below, the systems used in this study were optically transparent.

Unlike the measurement of the sediment layer thickness, however, the determination of the particle velocity and concentration profiles within flowing concentrated suspensions presents a much more difficult challenge and various attempts were made over the years to develop, for this purpose, several non-intrusive experimental techniques. One of the earliest was described by Karnis, Goldsmith & Mason (1966), who employed cinematography to visualize the motion of tracer particles within the flow and thereby were able to estimate the particle velocity and the concentration profiles within concentrated suspensions flowing in a tube. Later on, more sophisticated techniques based on the Doppler effect phenomenon were developed by number of investigators to study flows of concentrated suspensions. Most of these methods, however, were restricted to the measurement of velocity profiles within such suspensions. For example, microwave Doppler anemometry (McMahon & Parker 1975) and ultrasound Doppler anemometry (Kowalewski 1980) were developed to measure the velocity profiles within the highly concentrated suspensions, but both these methods fail to provide the spatial resolution needed for the present application. The well known laser Doppler velocimetry (LDA), which is capable of providing an extremely high spatial resolution compared to the other two even though it requires that the medium be optically transparent, was also employed (Nouri, Whitelaw & Yianneskis 1987) to measure particle velocities in relatively dilute suspensions with concentrations up to 14%, by matching the refractive index (RI) of the particles to that of the fluid. Since, in practice, it is extremely difficult to make a suspension completely transparent owing to the residual turbidity that arises from the slight mismatch in the refractive indices as well as the presence of impurities within the particles, the application of this technique to a particular system depends strongly on the degree of transparency that can be achieved by matching the refractive indices. This in turn determines the beam penetration distance within which the velocity could be measured for a given volume fraction of particles.

Recently, however, Koh (1991) and Koh *et al.* (1994) have shown that, in addition to measuring the particle velocities, this technique can also be extended to yield particle concentration profiles in flowing concentrated suspensions by counting the number of scattering centres crossing the measuring volume. Clearly, this is possible only when each scattering centre gives rise to a distinct burst. This can be achieved by keeping the size of the measuring volume smaller than the particle size. Nevertheless, beyond a certain combination of particle volume fractions and beam penetration distances, the residual turbidity of the system increases and the quality of Doppler burst deteriorates significantly thereby rendering the processing of these signals extremely difficult. Specifically, for the system employed by Koh (1991), this limit was reached at an average volume fraction of 30% and with a beam penetration distance of around 50 particle diameters, at which point these investigators reported a large scatter in their velocity data, due to the low signal to noise ratio of the Doppler signal. In turn this made it impossible for them to obtain reliable particle concentration measurements under these conditions. In principle, these restrictions can be overcome by employing a technique based on the NMR imaging which was recently used by several investigators (Graham *et al.* 1991; Sinton & Chow 1991) to measure the velocity as well as concentration profiles within concentrated suspensions, but, owing to the high capital cost of the NMR equipment, this method does not provide a viable alternative for the present application.

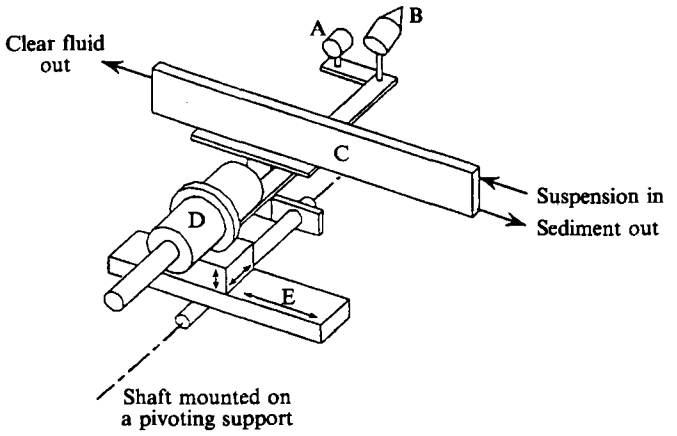

FIGURE 8. Schematic description of the experimental set-up. A: video camera, B: PM tube connected to a BSA, C: low aspect ratio settling vessel, D: laser Doppler anemometer, E: x, y, z table.

Instead, by employing an advanced burst processing system and a better optical configuration in addition to matching the refractive index of the particles to that of the fluid, we were able to extend the LDA technique and thereby measure the particle velocities within highly concentrated sediment layers having particle volume fractions as high as 50% and at locations as far as 100 particle diameters inside the flow. Unfortunately, under these conditions the Doppler burst does not remain distinct and the validation rate through the processor depends significantly on the signal to noise ratio of the signal and thereby on the medium through which the incident beams and the scattered signals are traversing. It was not possible, therefore, to compare the number of scattering centres passing through the measuring volume at two different locations and thereby obtain meaningful concentration data from these measurements. We also note that the determination of the particle concentration using this technique under such extreme conditions requires that a careful study be made of the effect of the optical turbidity, which arises from the slight mismatch in the refractive indices on the Doppler bursts, and, more specifically, that the one to one correspondence between the particles crossing the measuring volume and the signals received at the PM tube be first established.

In addition, and in contrast to the case of a flowing pure fluid, the adaptation of LDA to the measurement of velocities in concentrated suspensions gives rise to several sources of error. First of all, as mentioned earlier, at high particle concentrations, the existence of many particles in the probe volume introduces noise into the scattered signal and may result in erroneous velocity readings. This error can be reduced by making the measuring volume nearly the same as that of the particle and can also be minimised to some extent by employing an appropriate signal processing technique which discards signals from multiple particles. The second source of error in the measurement of the velocity is due to the changes in the refractive index of the medium encountered by the laser beam. Thus, the resulting wobble of the beam can introduce noise into the velocity signal akin to fictitious turbulence. This source of error, however, cannot be removed completely since, in practice, a small amount of mismatch always exists even when the refractive indices of the fluid and of the particles are matched in a suspension.

	Density (gm cm^{-3})	Viscosity (cP)	Refractive index at 24 °C
Turpentine	0.85	1.43	1.4636
Tetraline	0.97	2.01	1.5388
Suspending fluid, mixture of 62.9% turpentine and 37.1% tetralin	0.89	1.47	1.4908
Particles, Acrylic, average diameter 90 μm (variance = ±8 μm)	1.18	—	1.491

TABLE 1. Physical properties of the fluid and particles used

4.1. *Experimental set-up*

The experimental set-up used in the present investigation and shown schematically in figure 8 consisted of a settling vessel of dimensions 25 in. (L) × 1 in. (W) × 2.5 in. (H), which was connected to the flow system mounted on a pivoting stand so that it could be rotated to the desired angle of inclination. A laser Doppler anemometer and a video camera for measuring the particle velocities and the sediment layer thickness respectively, with a resolution of 10 μm in all three directions, was attached to an x, y, z table which was fixed to the same pivoting shaft that was holding the settling vessel.

As mentioned earlier, the application of LDA to concentrated suspensions requires that the suspension be optically transparent, which in general can be achieved by matching the refractive indices of particles to that of the fluid. There are of course several factors which affect the optical quality of the suspensions, namely the refractive indices of the two phases, the optical quality of the particles and the impurities and non-uniformity present in the solid phase. In addition, the proposed theoretical model also requires that the particles be spherical and monodisperse. These restrictions posed a major constraint in choosing the appropriate fluid–particle system for the experiments. However, in the present case, a careful inspection of a variety of polymer and resin samples from different manufacturers led us to choose a class of PMMA beads (CA603) manufactured by ICI, which were found to contain only a very small number of air bubbles and hence were most suited for our application. These particles were spherical but, owing to their wide size distribution, had to be sieved. The density of these particles was found to be 1.178 gm cm^{-3}. For PMMA, the refractive index is approximately 1.491; however, the actual RI of the particles used in the experiments, an important parameter for the refractive index matching, was not available from the manufacturer. Following Koh (1991), who presented a number of methods then available for RI matching, a systematic procedure was adopted for matching the refractive index of particles with that of the suspending fluid which did not require that the RI of the particles be known prior to matching. Clearly, this is possible in practice only when the suspending fluid is prepared by mixing two or more fluids so that its refractive index can be changed by varying its composition. A mixture of turpentine and tetraline was therefore chosen and its proper composition was arrived at by maximizing the transmittance of the suspension. The physical properties of the fluid–particle system used are given in table 1. Moreover, since the refractive indices of both phases depend strongly on the temperature, it was necessary that the RI matching as well as all the other experiments be performed at the same temperature. As pointed out by Koh (1991) and also found during the course of our experiments, it is essential that temperature control be maintained; however, in practice, control to within 1 °C was found to be sufficient for our purposes.

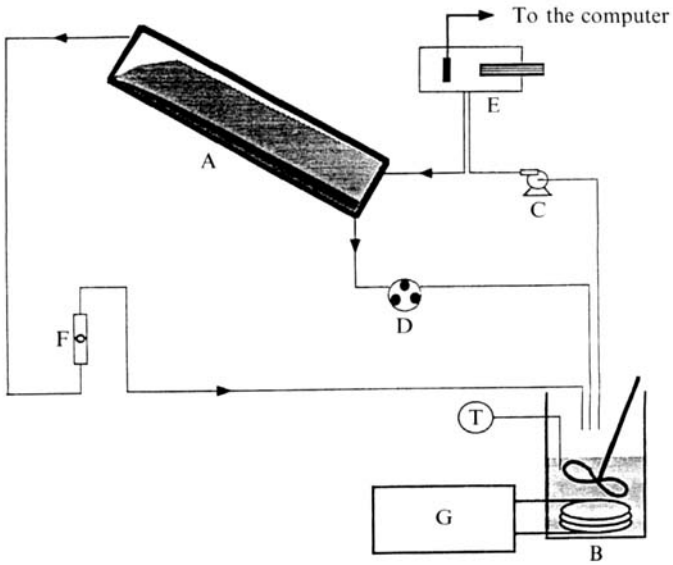

FIGURE 9. Schematic representation of the flow system. A: flow vessel, B: mixing tank, C: centrifugal pump, D: peristaltic pump, E: concentration measurement system, F: flow meter, G: temperature-controlled bath; T: digital thermometer.

The details of the flow system are shown schematically in figure 9. The overflow product and the sediment that were withdrawn from the vessel were eventually remixed in the mixing chamber which was equipped with a mechanical stirrer and cooling coils to maintain a constant temperature. The temperature of the suspension in the mixing tank was monitored by means of a thermistor probe and was controlled manually by changing the set point of the temperature of the water within the circulator bath which circulated through the cooling coils of the mixing tank. The rate of the overflow product at the top of the vessel was measured using a flowmeter. The volumetric concentration of the particles in the feed was determined by measuring, using a photodiode, the transmittance of a laser beam through the suspension flowing in a cell. In addition, the particle volume fraction within the suspension region of the flow channel was checked at several locations by the same technique and was found to match the inlet concentration to within 1%.

The laser Doppler anemometer used for the particle velocity measurements was a one-dimensional system equipped with a 15 mW He–Ne laser and a Bragg cell. It was used in the off-axis forward scattering mode in order to maximize the signal to noise ratio of the scattered signal. The optics for this system were obtained from Dantec Electronics and were chosen in such a way that the measuring volume was smaller than the size of suspending particles. Thus, in the present work, by means of a beam expander and a front lens of focal length 80 mm, we constructed a measuring volume of size $d_x = 41$ μm, $d_y = 41$ μm and $d_z = 249$ μm. In addition, a set of close-up lenses connected to a photomultipler (PM) tube was placed in the forward direction, as shown in figure 8 and was used for focusing the collected light into a PM tube through a pinhole. The output of this PM tube was connected to an on-line processor with a built-in FFT chip, developed by Dantec and called a Burst Spectrum Analyzer (BSA). This BSA employed an advanced burst detection scheme to accurately find and validate the burst and was capable of processing signals with a signal to noise ratio as low as -6 dB. A personal computer was interfaced by IEEE488 with the BSA to

obtain the data, which consisted of the velocity, the transit time and the arrival time of each burst processed. At each point one thousand bursts were processed and the average velocity was then calculated by taking the arithmetic mean of these bursts. In addition, in few cases, the transit times were used to weigh these averages, but the difference between these two sets were found to be negligible. The data were stored in the computer and were analysed at the end of an experiment to obtain the particle velocity distribution at each point.

In addition, a video system, consisting of a video camera (Sony XC77RR) along with a VCR (Panasonic AG1960) and a Sony monitor, was attached to the experimental system in order to visually observe and measure the thickness of the steady flowing sediment layer. The latter was done manually from the monitor which reproduced the image of the sediment layer magnified 35 times its actual size.

5. Comparison with the theory

Visual observations of the flowing sediment layer clearly indicated a sharp change in the contrast around the sediment–suspension interface, thereby confirming the theoretical prediction about the jump in particle concentration across the suspension–sediment interface. As described earlier in the previous section, this feature of the sediment layer made it possible to measure the sediment layer thickness by means of video imaging. Furthermore, in order to verify the second quantitative prediction of the model, we measured the velocity of the particles within the sediment layer at various x-positions, and the y-locations at which the longitudinal velocities reached their maximum values were found to almost coincide with the corresponding locations where the sharp change in the visual contrast was observed.

In the present work, experiments were performed for four feed particle concentrations and for two angles of inclination, and the measured sediment layer thickness profiles plus some typical particle velocity profiles for each of these cases were compared with the corresponding theoretical predictions based on the theory presented in §§2 and 3. Figures 10(*a*)–10(*c*) show some typical experimentally measured sediment layer thickness profiles along with the corresponding theoretical predictions which are depicted as solid lines. Clearly, there is a good agreement between the theory and experiments. It should be noted that most of the experimental data were restricted to values of $\tilde{x} < 230$ mm, primarily because the visual identification of the interface became difficult at larger $\tilde{x}$ due to the high velocity of the particles. The corresponding predictions of the original no-slip theory by Nir & Acrivos (1990) are not shown in these figures because they exceeded the measured thicknesses by more than 150%.

The particle velocity profiles for various feed particle concentrations and $\tilde{x}$-locations are shown in figures 11(*a*)–11(*e*) which also contain plots of the corresponding theoretical predictions for the particle concentration profile. Unfortunately, owing to the lack of any experimental measurements, the latter could not be compared with experiments. A solid line in these plots represents the theoretically predicted profiles, while the dashed line refers to the corresponding predictions based on the no-slip theory of Nir & Acrivos (1990) modified to include the effects of shear-induced diffusion due to shear stress gradients. As described earlier, on comparing the two sets of figures 10 and 11(*a–c*), it seems that, as predicted theoretically, the location of the maximum in the measured velocity profile almost coincides with the location of the sediment–suspension interface as determined optically. Also, the velocity profiles in these figures clearly point to the existence of a slip velocity close to the inclined plate, which is consistent with visual observations that were made during the course of our

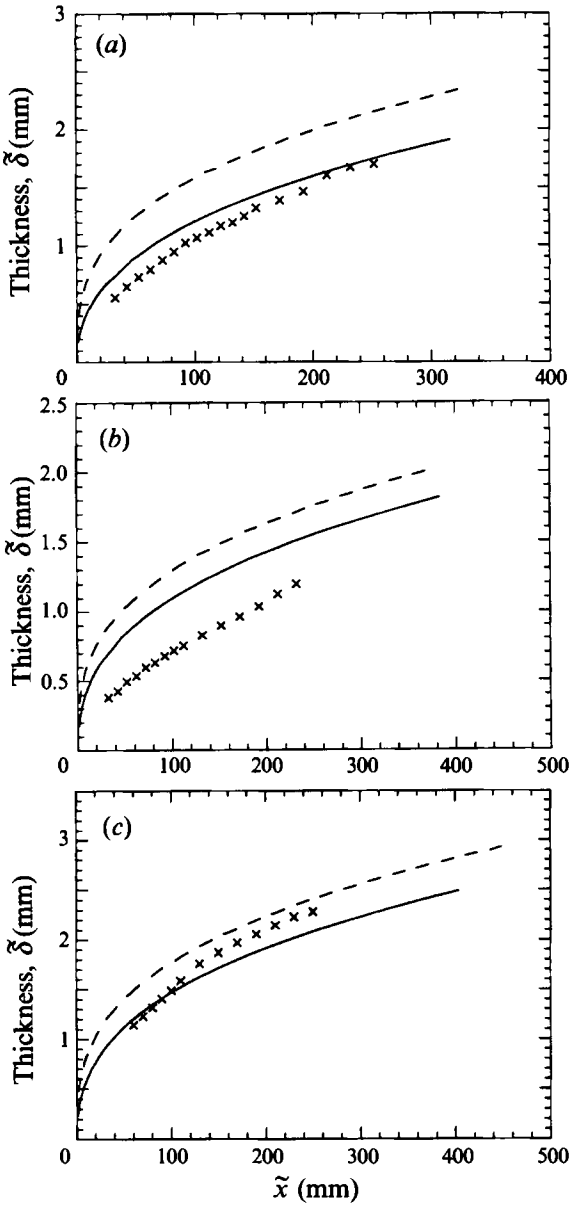

FIGURE 10. Sediment layer thickness profile for (*a*) $\phi_s = 6.5\%$ and $\theta = 35°$; (*b*) $\phi_s = 9.6\%$ and $\theta = 45°$; (*c*) $\phi_s = 12.0\%$ and $\theta = 35°$. ——, Theory; – – –, theory without slip; ×, experimental points.

experiments. It was not possible, however, to measure particle velocities any closer than 0.25 mm from the plate due to saturation of the PM tube current caused by the presence of excessive reflections from the wall. In fact, this is one of the reasons which contributed to the large scatter in the particle velocities measured close to the wall. Furthermore, the low values of these velocities also made it difficult to separate the actual signal from the noise that could have been present due to external vibrations and the optical turbidity of the medium. Therefore, in order to avoid these spurious signals, most of the velocity profiles were measured at a distance far away from the origin, i.e.

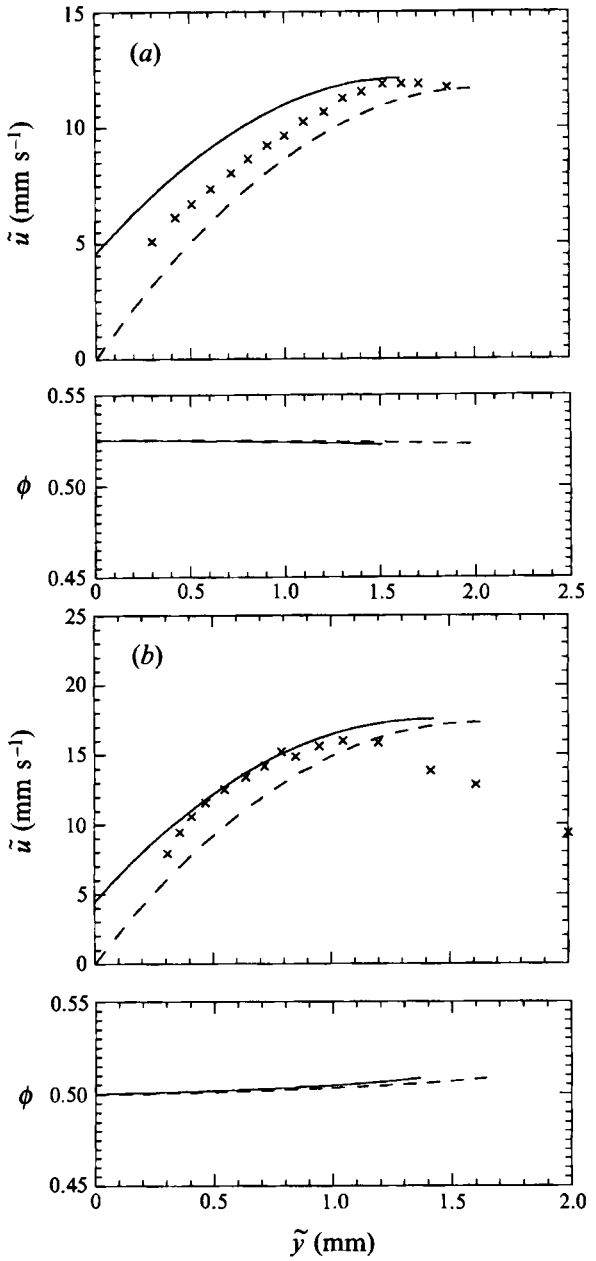

FIGURE 11(*a*, *b*). For caption see page 63.

$\tilde{x} > 180$ mm, where the sediment layer was relatively thick and the particle velocities relatively high. It should be noted at this point that, although all the velocity data shown in figure 11(*a–e*) correspond to particle velocities measured within the sediment layer, owing to the relatively small magnitude of the settling velocity and therefore of the slip velocity of the particles relative to the bulk, the data also depict, for all practical purposes, the bulk velocities within the sediment layer.

Furthermore, the velocity measurements shown in figure 11(*a–e*) clearly indicate that a strong velocity gradient exists within the sediment layer, especially for higher values of

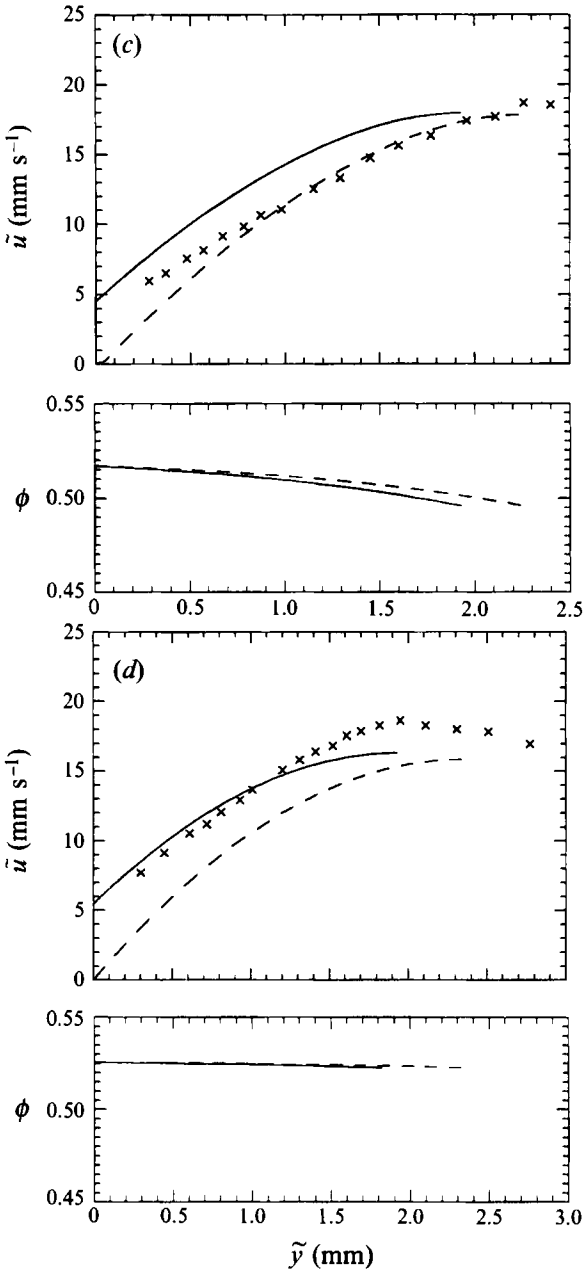

FIGURE 11(*c*, *d*). For caption see facing page.

the feed particle concentration and large angles of inclination. Another interesting feature of these profiles is that almost all the plots are linear over the entire range of the sediment layer except for a small region close to the interface where the velocity attains its maximum value. In view of the momentum balance equation (12), this suggests the existence of a non-uniform particle concentration distribution within the sediment layer with concentration gradients of the order $(d\lambda/d\phi)^{-1}$. Clearly, this is very small for most of the cases shown in these figures since ϕ is close to ϕ_s under these conditions and provides further evidence that the approximate solution to be presented

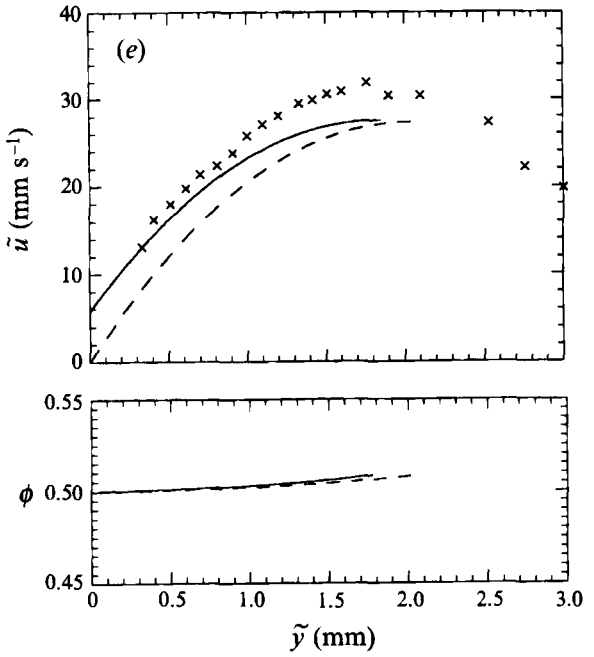

FIGURE 11. Experimentally measured (×) and theoretically predicted velocity profiles within a sediment layer and calculated particle concentration profiles at (*a*) $\tilde{x} = 204$ mm, for $\phi_s = 6.5\%$ and $\theta = 35°$; (*b*) $\tilde{x} = 204$ mm, for $\phi_s = 9.6\%$ and $\theta = 45°$; (*c*) $\tilde{x} = 204$ mm, for $\phi_s = 12.0\%$ and $\theta = 35°$; (*d*) $\tilde{x} = 324$ mm, for $\phi_s = 6.5\%$ and $\theta = 35°$; (*e*) $\tilde{x} = 404$ mm, for $\phi_s = 9.6\%$ and $\theta = 45°$. ——, Theory with slip; – – –, theory without slip.

in the Appendix should give results in close agreement with those arrived at via the numerical solution of the full model equations.

The main conclusion to be drawn from the foregoing comparison is that there exists, in most cases, surprisingly close agreement between experiments and theory, especially considering that the latter did not entail the use of any adjustable parameters.

This research was supported in part by the National Science Foundation under grants CTS-8896170 and CTS-9012546 and the Department of Energy under grants DE-FG02-90-ER14139. Special thanks are due to Mr Robert Suhoke Jr for his expert help in the design of the experimental setup and in setting up the LDA. We also wish to thank Mr Anubhav Tripathi for repeating some of the calculations and experiments as well as Mr I. Ortiz and Mr Z. R. Xu for machining the experimental apparatus.

Appendix

In this Appendix we shall present approximate expressions for the sediment layer thickness $\delta(x)$ and for the longitudinal velocity profile, both transformed according to (11), when the particle volume fraction within this layer is set equal to ϕ_δ. To begin with, on account of this approximation, the velocity profile within the sediment layer can be easily obtained from the momentum balance equation (12) subject to the boundary conditions (14) and (16), as

$$U = \frac{9}{2\lambda(\phi_\delta)}(\phi_\delta - \phi_s)\{\delta(X) + Y\delta(X) - \tfrac{1}{2}Y^2\}\sin\theta, \tag{A 1}$$

		δ_0		δ_∞	
ϕ_s	θ	From the small-X asymptotic solution	From equation (A 3)	From the large-X asymptotic solution	From equation (A 4)
0.05	30	3.162	2.719	3.099	2.812
	45	1.463	1.998	1.863	2.289
	60	0.735	1.491	1.179	1.884
0.10	30	3.611	2.628	3.385	2.748
	45	1.917	2.076	2.208	2.349
	60	1.086	1.661	1.529	2.024
0.15	30	4.133	2.573	3.703	2.709
	45	2.293	2.094	2.505	2.362
	60	1.365	1.737	1.779	2.085
0.20	30	4.910	2.590	4.155	2.723
	45	2.743	2.131	2.817	2.390
	60	1.663	1.800	2.026	2.135

TABLE 2. Comparison between the asymptotic solutions described in §2 and the approximate solution shown in the Appendix

where, as before $\delta(X)$ represents the sediment layer thickness at any location X. In addition, in applying (14), q has been set equal to unity by choosing $\zeta = \zeta_c(\phi_\delta)$. But, in view of the above expression for U and the flux matching condition (17) at the interface $Y = \delta(X)$, one obtains that

$$\tfrac{1}{3}\delta^3 + \delta^2 = \left[\frac{2\lambda(\phi_\delta)}{9(\phi_\delta - \phi_s)^2 \tan\theta}(\phi_s f(\phi_s) - \phi_\delta f(\phi_\delta)) + \frac{\alpha(\phi_\delta)}{(\phi_\delta - \phi_s)}\right] X, \tag{A 2}$$

where use has been made of the continuity equation to obtain the expression for V_δ. Clearly, when $\delta \ll 3$, (A 2) reduces to

$$\delta = \left[\frac{2\lambda(\phi_\delta)}{9(\phi_\delta - \phi_s)^2 \tan\theta}(\phi_s f(\phi_s) - \phi_\delta f(\phi_\delta)) + \frac{\alpha(\phi_\delta)}{(\phi_\delta - \phi_s)}\right]^{1/2} X^{1/2}, \tag{A 3}$$

consistent with the form of the small-X asymptotic solution. On the other hand, when $\delta \gg 3$,

$$\delta = \left[\frac{2\lambda(\phi_\delta)}{3(\phi_\delta - \phi_s)^2 \tan\theta}(\phi_s f(\phi_s) - \phi_\delta f(\phi_\delta)) + 3\frac{\alpha(\phi_\delta)}{(\phi_\delta - \phi_s)}\right]^{1/3} X^{1/3}, \tag{A 4}$$

which again has the correct dependence on X as the large X-solution. Table 2 compares the coefficients δ_0 and δ_∞ of the asymptotic expressions $\delta = \delta_0 X^{1/2}$ and $\delta = \delta_\infty X^{1/3}$ for $X \to 0$ and $X \to \infty$, respectively, as obtained from the numerical solution of the similarity equations derived in §2, to those computed using (A 3) and (A 4). Clearly, there is fair agreement between these two solutions, especially at the higher values of ϕ_s and the higher angles of inclination.

It is important to emphasize that this approximate analysis in no way discards the influence of shear-induced particle diffusion since the expression for $\delta(X)$ given by (A 3) and (A 4) both involve the coefficients $\alpha(\phi)$ and $\beta(\phi)$, either explicitly as in the case of α or implicitly through the dependence of ϕ_δ on these two functions, cf. (21) and (22). Rather, as a consequence of the assumption of a uniform particle volume fraction ϕ_δ, a simple expression for the longitudinal velocity profile could be derived via (12) which, on account of (17), led directly to (A 2). Thus, the role played by shear-induced

particle diffusion remains a key ingredient of both the more exact as well as the approximate analysis presented above.

REFERENCES

ACRIVOS, A. & CHANG, E. 1986 A model for estimating transport quantities in two-phase materials. *Phys. Fluids* **29**, 3–4.

ACRIVOS, A. & HERBOLZHEIMER, E. 1979 Enhanced sedimentation in settling tanks with inclined walls. *J. Fluid Mech.* **92**, 435–457.

BRADY, J. F. & BOSSIS, G. 1988 Stokesian dynamics. *Ann. Rev. Fluid Mech.* **20**, 111–157.

CHANG, E. Y. & ACRIVOS, A. 1987 Conduction of heat from a planar wall with uniform surface temperature to a monodisperse suspension of spheres. *J. Appl. Phys.* **62**, 771–776.

DURLOFSKY, L. J. & BRADY, J. F. 1989 Dynamic simulation of bounded suspensions of hydrodynamically interacting particles. *J. Fluid Mech.* **200**, 39–67.

GRAHAM, A. L., ALTOBELLI, S. A., FUKUSHIMA, E., MONDY, L. A. & STEPHENS, T. S. 1991 NMR imaging of shear-induced diffusion and structure in concentrated suspensions. *J. Rheol.* **35**, 191–201.

HERBOLZHEIMER, E. & ACRIVOS, A. 1981 Enhanced sedimentation in narrow tilted channels. *J. Fluid Mech.* **108**, 485–499.

JANA, S. C., KAPOOR, B. & ACRIVOS, A. 1995 Apparent wall slip velocity coefficients in concentrated suspensions of non-colloidal particles. *J. Rheol.* (submitted).

KAPOOR, B. 1994 Flow of a sediment layer on an inclined plate. PhD dissertation, The City University of New York.

KARNIS, A., GOLDSMITH, H. L. & MASON, S. G. 1966 The kinetics of flowing dispersions: I. Concentrated suspensions. *J. Colloid Sci.* **22**, 531–553.

KOH, C. J. 1991 Experimental and theoretical studies on two phase flows. PhD dissertation, California Institute of Technology.

KOH, C. J., HOOKHAM, P. & LEAL, L. G. 1994 An experimental investigation of concentrated suspension flows in a rectangular channel. *J. Fluid Mech.* **266**, 1–32.

KOWALEWSKI, T. A. 1980 Velocity profiles of suspensions flowing through a tube. *Arch. Mech.* **32**, 857–865.

LEIGHTON, D. & ACRIVOS, A. 1986 Viscous resuspension. *Chem. Engng Sci.* **41**, 1377–1384.

LEIGHTON, D. & ACRIVOS, A. 1987*a* Measurement of shear-induced self-diffusion in concentrated suspensions of spheres. *J. Fluid Mech.* **177**, 109–131.

LEIGHTON, D. & ACRIVOS, A. 1987*b* The shear-induced migration of particles in concentrated suspensions. *J. Fluid Mech.* **181**, 415–439.

LEUNG, W. F. & PROBSTEIN, R. F. 1983 Lamella and tube settlers 1. Model and operation. *Ind. Engng Chem. Proc. Des. Rev.* **22**, 58–67.

MCMAHON, T. A. & PARKER, R. R. 1975 Particles in tube flow at moderate Reynolds number. *Trans. Soc. Rheol.* **19**, 445–456.

NIR, A. & ACRIVOS, A. 1990 Sedimentation and sediment flow on inclined surfaces. *J. Fluid Mech.* **212**, 139–153.

NOURI, J. M., WHITELAW, J. H. & YIANNESKIS, M. 1987 Particle motion and turbulence in dense two-phase flows. *Intl J. Multiphase Flow* **13**, 729–739.

PHILLIPS, R. J., ARMSTRONG, R. C. & BROWN, R. A. 1992 A constitutive equation for concentrated suspensions that accounts for shear-induced particle migration. *Phys. Fluids* A **4**, 30–40.

PROBSTEIN, R. F., YUNG, R. & HICKS, R. 1981 In *Physical Separations* (ed. M. P. Freeman & J. A. Fitzpatrick), pp. 53–92. New York: Engineering Foundation.

RUBINSTEIN, I. 1980 A steady laminar flow of a suspension in a channel. *Intl J. Multiphase Flow* **6**, 473–490.

SCHAFLINGER, U., ACRIVOS, A. & ZHANG, K. 1990 Viscous resuspension of a sediment within a laminar and stratified flow. *Intl J. Multiphase Flow* **16**, 567–578.

SCHNEIDER, W. 1982 Kinematic-wave theory of sedimentation beneath inclined walls. *J. Fluid Mech.* **120**, 323–346.

SHAQFEH, E. S. G. & ACRIVOS, A. 1986 The effect of inertia on the buoyancy driven convection flow in settling vessels having inclined walls. *Phys. Fluids* **29**, 3935–3948.

SHAQFEH, E. S. G. & ACRIVOS, A. 1987 The effects of inertia on the stability of the convective flow in inclined particle settlers. *Phys. Fluids* **30**, 960–973.

SINTON, S. W. & CHOW, A. W. 1991 NMR flow imaging of fluids and solid suspensions in Poiseuille flow. *J. Rheol.* **35**, 735–772.